Hydration Effects on Reaction Profiles: An ab Initio Dielectric Continuum Study of the S_N2 $Cl^- + CH_3Cl$ Reaction

Thanh N. Truong* and Eugene V. Stefanovich†

Department of Chemistry, University of Utah, Salt Lake City, Utah 84112

Received: June 9, 1995; In Final Form: July 24, 1995⊗

We present ab initio studies of the hydration effects on the reaction profile of the S_N2 $Cl^- + CH_3Cl$ reaction using our recently proposed generalized conductor-like screening model (GCOSMO) within the quantum mechanical and classical frameworks including both electrostatic and nonelectrostatic contributions to the hydration free energy. For the quantum mechanical approach, we employed the Hartree−Fock (HF), second-order Møller−Plesset perturbation theory (MP2), and hybrid nonlocal density functional theory (DFT) with the 6-31+G(d,p) basis set. Using the GCOSMO model, we found that the calculated free energy reaction profile of the title S_N2 reaction in aqueous solution is in good agreement with experimental observations and previous studies. The solvent reaction field was found to have a noticeable effect on the solute electronic density distribution. The DFT free energies of hydration agree very well with MP2 results and are in better agreement with experimental data than HF results. The DFT-GCOSMO approach provides a promising tool for studies of mechanisms of chemical and biochemical reactions in solutions.

I. Introduction

The $Cl^- + CH_3Cl$ bimolecular nucleophilic substitution (S_N2) reaction in the gas phase and aqueous solution has been widely studied both theoretically and experimentally due to its important role in physical organic chemistry.[1−5] In particular, hydration effects are known to lower the transfer rate by 20 orders of magnitude. Although the reaction profile of the S_N2 reaction has a double well form in the gas phase,[6] it is believed to be unimodal in an aqueous environment.[7] Due to such dramatic effects of the solvent on the reaction profile and rates, this reaction has often been used as a prototype reaction for testing the accuracy and efficiency of newly developed solvation theories such as our recently proposed generalized conductor-like screening model (GCOSMO).[8,9]

There have been numerous theoretical studies[10−14] on the potential energy surface of the gas-phase $Cl^- + CH_3Cl$ reaction. The most accurate ab initio molecular orbital study to date was done by Glukhovtsev et al.[15] at the G2(+) level of theory. Another recent study by Deng et al.[14] provided a critical analysis on the performance of density functional theory (DFT) in calculating both the equilibrium and transition-state properties of the gas-phase S_N2 reactions, $X^- + CH_3X$ for X = F, Cl, Br, and I. These authors found that both the local Vosko−Wilk−Nusair[16] (VWN) and nonlocal Becke[17]−Perdew[18] (BP) DFT methods noticeably underestimate the barrier heights. This study, however, did not include hybrid Hartree−Fock−DFT methods, such as the combination of Becke's three-parameter exchange[19] with Lee−Yang−Parr (LYP) correlation[20] (B3LYP) or the combination of Becke's half-and-half exchange[21] with LYP correlation (BH&HLYP) methods. Both of these hybrid DFT methods have been found previously to give more accurate transition state information than BP or BLYP methods.[22−27]

Most theoretical efforts[2,28−48] in understanding hydration effects in chemical reactions generally can be categorized into three different approaches. One approach is the use of *classical* molecular dynamics (MD) or Monte Carlo (MC) methods with explicit treatment of solvent molecules.[30,34,35,37,38,41,47] However, when using these methodologies, the effective atomic charges of the solute used in the determination of the solute−solvent electrostatic interaction are often taken from the gas-phase electronic structure calculations, and thus the solvent effect on the solute electronic density distribution is not included. This effect can be important in charge-transfer reactions such as in the $Cl^- + CH_3Cl$ reaction, though this has not been well addressed. Recent combined quantum mechanics/molecular mechanics approaches[31,32,49] can include this effect and offer promising alternatives for classical MD or MC simulations of reactions in solution. The influence of the solvent reaction field on the electronic structure of the solute can be modeled approximately by using either a *supermolecule* or *continuum* model. The supermolecule approach represents the local solute−solvent interaction by a small number of nearest-neighbor solvent molecules and has been employed to study S_N2 reaction in hydrated clusters.[28,40,42] This approach includes the effect of the hydrogen bonding between the solute and nearby solvent molecules; however, it cannot account for the effect of the long-range electrostatic interaction with the bulk solvent. In the continuum approach, a solvated system is modeled by the solute inside a cavity surrounded by a dielectric continuum medium. Even though this approach models the solvent by a single parameter, namely, the dielectric constant ϵ, it appears to offer considerable promise for applications in chemical, biological, and pharmacological areas. In particular, it has been used to study the S_N2 reactions.[39,43−46,48]

Recently, we have introduced a new dielectric continuum solvation model, the generalized conductor-like screening model (GCOSMO), and incorporated it into classical, ab initio molecular orbital and density functional theory frameworks.[8,9] This model is a generalization of the semiempirical COSMO model proposed by Klamt and Schüürmann.[50] The original COSMO model calculates the electrostatic solvation energy by representing the solute charge distribution as a set of point charges and dipoles in the neglect differential diatomic overlap formalism. The GCOSMO model not only has a general description of the solute charge density but also includes the dispersion, repulsion and cavity formation contributions. An advantage of both

* To whom all correspondence should be addressed.
† On leave from the Institute of Chemical Physics, University of Latvia, 19 Rainis blvd, Riga LV1586, Latvia.
⊗ Abstract published in *Advance ACS Abstracts,* September 1, 1995.

0022-3654/95/2099-14700$09.00/0

COSMO and GCOSMO models is that the solvent effects on the solute electron density are included directly as additional terms to the Hartree−Fock−Roothaan matrix elements. This allows convergence of both the solute electronic wave function and the solvent reaction field in the same SCF cycle and analytical energy derivatives have simple expressions.[50,51] As a result, the computational demand was found to be on the average only 10% more than for the gas-phase calculations. We have tested our solvation model for a number of ions and neutral polar molecules and found that the accuracy in the calculated hydration free energy is comparable to that of the well-known polarizable continuum model[52,53] (PCM) or the combined DFT with the Poisson−Boltzmann formalism (DFT/PB) model.[54−56] Furthermore, in a recent study,[8] we have found that GCOSMO is more stable than the PCM model with respect to the location of the solute inside the cavity and positions of the surface charges.

Our present study has two objectives, namely, (1) to provide a deeper understanding in the hydration effects on the S_N2 reaction profile, in particular, we focus on the importance of electrostatic and nonelectrostatic contributions to the hydration free energy, the effect of the solute electron correlation on the hydration energy and the effect of the solvent on the solute electron distribution, and (2) to test the accuracy of our GCOSMO model for predicting the reaction profile of the S_N2 $Cl^- + CH_3Cl$ reaction in an aqueous solution and to compare the performance of GCOSMO with the recent implementation of the PCM model in the Gaussian 94 program. In the following section, we give an overview of the GCOSMO solvation model. Section III provides computational details. The results are presented and discussed in section IV, and conclusions are given in section V.

II. Generalized Conductor-like Screening Model (GCOSMO)

The essence of the GCOSMO method[9] is first to define the surface charge density $\sigma(\mathbf{r})$ on the surface (S) of the cavity for a screening conductor (the dielectric constant $\epsilon = \infty$) from a boundary condition that the electrostatic potential on the surface S is zero:

$$\sum_i \frac{z_i}{|\mathbf{r} - \mathbf{R}_i|} - \int_V \frac{\varrho(\mathbf{r}')}{|\mathbf{r} - \mathbf{r}'|} d^3r' + \int_S \frac{\sigma(\mathbf{r}')}{|\mathbf{r} - \mathbf{r}'|} d^2r' = 0 \quad (1)$$

where $\mathbf{r}$ is on S, ϱ is the solute electron density, and z_i is the nuclear charge of an atom i. For a dielectric medium specified by the dielectric constant ϵ, the surface charge density is then determined approximately by scaling the screening conductor surface charge by a constant factor, $f(\epsilon) = (\epsilon - 1)/\epsilon$, to satisfy Gauss's theorem for total surface charge. This approach yields an error of order ϵ^{-1} in the solvation energy. Such error is negligible for the aqueous solvent where the dielectric constant is 80.[8]

In our approach, we use the solvent-excluding surface as defined by Richards[57] and the boundary element method to define the cavity boundary. The boundary is defined by M surface elements with areas $\{S_u\}$ and the surface charge density at each surface element is approximated as a point charge, $\{q_u\}$, located at the center of that element, $\{\mathbf{t}_u\}$. From eq 1, the surface charge distribution is given by

$$\mathbf{q} = -f(\epsilon)\mathbf{A}^{-1}(\mathbf{Bz} + \mathbf{c}) \quad (2)$$

where $\mathbf{A}$, $\mathbf{B}$, and $\mathbf{c}$ are M × M, M × N, and M × 1 matrixes, respectively, with matrix elements defined by[50]

$$A_{uv} = \frac{1}{|\mathbf{t}_u - \mathbf{t}_v|} \quad \text{for } u \neq v, \text{ and } A_{uu} = 1.07\sqrt{4\pi/S_u} \quad (3)$$

$$B_{ui} = \frac{1}{|\mathbf{t}_u - \mathbf{R}_i|} \quad (4)$$

$$c_u = -\int \frac{\varrho(\mathbf{r})}{|\mathbf{r} - \mathbf{t}_u|} d^3r \quad (5)$$

and $\mathbf{z}$ is the vector of N nuclear charges. Alternatively, the surface charges can be determined by variationally minimizing the total electrostatic solvation energy

$$\Delta G_{\text{els}}(\mathbf{q}) = \mathbf{z}^\dagger\mathbf{B}^\dagger\mathbf{q} + \mathbf{c}^\dagger\mathbf{q} + \frac{1}{2f(\epsilon)}\mathbf{q}^\dagger\mathbf{Aq} \quad (6)$$

with respect to $\mathbf{q}$ († denotes matrix transposition).

From eq 6, we have derived the solvent contributions to the one- and two-electron terms of the Fock matrix, $F_{\mu\nu}$, that are expressed as[9]

$$H^s_{\mu\nu} = -f(\epsilon)\, \mathbf{z}^\dagger\mathbf{B}^\dagger\mathbf{A}^{-1}\mathbf{L}_{\mu\nu} \quad (7)$$

$$G^s_{\mu\nu} = -f(\epsilon)\mathbf{c}^\dagger\mathbf{A}^{-1}\mathbf{L}_{\mu\nu} \quad (8)$$

respectively, where the matrix $\mathbf{L}_{\mu\nu}$ is defined by

$$L^u_{\mu\nu} = -\left\langle \mu \left| \frac{1}{|\mathbf{r} - \mathbf{t}_u|} \right| \nu \right\rangle \quad (9)$$

The total energy of the whole system (solute + surface charges) is given by

$$E = {}^1/_2 \sum_{\mu\nu} P_{\mu\nu}(H_{\mu\nu} + F_{\mu\nu}) - {}^1/_2 f(\epsilon)\mathbf{z}^\dagger\mathbf{B}^\dagger\mathbf{A}^{-1}\mathbf{Bz} + E_{\text{n-n}} \quad (10)$$

where $P_{\mu\nu}$ is the density matrix element and $E_{\text{n-n}}$ is the solute nuclear−nuclear repulsion.

Apart from the electrostatic term, the total free energy of solvation also includes the dispersion (ΔG_{dis}), repulsion (ΔG_{rep}), and cavity formation (ΔG_{cav}) contributions:

$$\Delta G_s = \Delta G_{\text{els}} + \Delta G_{\text{dis}} + \Delta G_{\text{rep}} + \Delta G_{\text{cav}} \quad (11)$$

In eq 11, we did not include other nonelectrostatic contributions to the total free energy of solvation—such as an entropy change due to the solvent reorganization, an enthalpy change due to changes in the solute vibrational and rotational degrees of freedom, a charge transfer to the solvent, the nonelectrostatic components of the solute−solvent hydrogen bonding, etc. We assumed that these contributions can be effectively included in the atomic radii defining the cavity boundary.

For the dispersion and short range repulsion contributions, we adopted the Floris et al. method:[58]

$$\Delta G_{\text{disp}} = \varrho_{H_2O} \sum_i^N \sum_u^M \frac{2d_{i\text{H}} + d_{i\text{O}}}{3r_{iu}^6}(\mathbf{r}_{iu}\cdot\mathbf{n}_u)S_u \quad (12)$$

$$\Delta G_{\text{disp}} = -\varrho_{H_2O} \sum_i^N \sum_u^M \frac{2c_{i\text{H}} + c_{i\text{O}}}{9r_{iu}^{12}}(\mathbf{r}_{iu}\cdot\mathbf{n}_u)S_u \quad (13)$$

where ϱ_{H_2O} is the density number of water; $d_{i\text{H}}$, $c_{i\text{H}}$ and $d_{i\text{O}}$, $c_{i\text{O}}$ are dispersion and repulsion coefficients for interactions of the solute atom i with the solvent hydrogen and oxygen atoms, respectively, which were taken from the OPLS force field[59] for

TABLE 1: Geometrical Parameters of the Methyl Chloride, $Cl^-\cdots CH_3Cl$ Ion–Dipole Complex and S_N2 $[Cl\cdots CH_3\cdots Cl]^-$ Transition State (Bond Lengths in angstroms and Angles in degrees)

geometry	HF	MP2	MP2[a]	BP[a]	BH&HLYP	B3LYP	expt[b]
CH_3Cl (C_{3v})							
R_{CCL}	1.786	1.778	1.779	1.778	1.786	1.804	1.785
R_{CH}	1.078	1.085	1.089	1.095	1.081	1.089	1.090
∠HCCl	108.4	108.9	108.9	108.2	108.5	108.5	108.1
$Cl^-\cdots CH_3Cl'$ (C_{3v})							
R_{CCl}	3.363	3.257	3.266	3.098	3.210	3.193	
$R_{CCl'}$	1.824	1.807	1.808	1.835	1.827	1.856	
R_{CH}	1.074	1.081	1.084	1.089	1.077	1.085	
∠HCCl′	108.0	108.9	108.9	107.9	108.3	108.0	
$[Cl\cdots CH_3\cdots Cl']^-$ (D_{3h})							
R_{CCl}	2.396	2.311	2.316	2.342	2.348	2.375	
R_{CH}	1.062	1.069	1.072	1.080	1.066	1.074	

[a] 6-31++G(d,p) and TZ+2P basis sets were used for MP2 and BP calculations, respectively. Taken from ref 14. [b] Reference 69.

this study; $\mathbf{n}_u$ is the unit vector normal to the surface at the point $\mathbf{t}_u$ and directed inside the cavity; $\mathbf{r}_{iu}$ is the $(\mathbf{t}_u - \mathbf{R}_i)$ vector. The cavity size in this case was increased to account for the solvent-excluding region by adding 1.4 Å (radius of solvent water)[57] to the solute atomic radii.

The cavity formation term is the work required to create the cavity in the solvent. Here we employed the scaled particle fluid theory of Pierotti,[60] which was transformed by Huron and Claverie[61] into an atom–molecule-type formalism. In particular, ΔG_{cav} is given by

$$\Delta G_{cav} = \sum_{i=1}^{N} \{K_0 + K_1 a_{is} + K_2 a_{is}^2 + K_3 a_{is}^3\} \frac{S_i^{exposed}}{S_i} \qquad (14)$$

where K_i ($i = 0-3$) are functions of the temperature, pressure, density, and hard-sphere diameter of the solvent taken from the work of Huron and Claverie.[61] a_{is} is the atomic radius of atom i plus 1.4 Å—the radius of the water molecule. $(S_i^{exposed}/S_i)$ is the fraction of the exposed surface of the solute atom i.

III. Computational Details

Stationary points on the gas-phase potential energy surface, namely, the CH_3Cl molecule, $Cl^-\cdots CH_3Cl$ ion–dipole complex and $[Cl\cdots CH_3\cdots Cl]^-$ transition state, were fully optimized at the Hartree–Fock (HF), second-order Møller–Plesset perturbation theory (MP2), and B3LYP and BH&HLYP levels using the 6-31+G(d,p) basis set. The hybrid B3LYP and BH&HLYP methods used in this study are those implemented in the Gaussian 92/DFT program.[62] Normal-mode analyses were performed at these points using an analytical second derivative method. Though, a gradient-following technique would be more appropriate for calculating the reaction coordinate, many previous studies have used a simpler reaction coordinate R_c defined by Chandrasekhar et al.[30] as

$$R_c = R_{CCl'} - R_{CCl} \qquad (15)$$

where Cl′ is the leaving atom. In this case, for each fixed R_c value, the remaining geometric parameters were fully optimized in C_{3v} symmetry for the gas phase. To facilitate a direct comparison with previous studies[30,39,44,48] on this reaction, we used the reaction coordinate (eq 15) in our work.

The reaction profile for the $Cl^- + CH_3Cl$ reaction in an aqueous environment was calculated at the HF, MP2, BH&HLYP, and B3LYP levels of theory using the GCOSMO model with the same 6-31+G(d,p) basis set and gas-phase geometries. Atomic radii for H, C and Cl (1.16, 2.30, and 1.937 Å, respectively) were taken from our previous work.[9] These atomic radii resemble to those used by Rashin and Namboodiri[63] (1.16, 2.46, and 1.937 Å, respectively) and in existing molecular mechanics OPLS,[59] CVFF,[64] and CHARMM[65] force fields. These atomic radii give rather accurate values of the hydration free energies for a large set of molecules. Solvent excluding surfaces were generated by using the GEPOL93 program.[66] To compare our results with the recent implementation of the polarizable continuum model (PCM) in the Gaussian 94 program,[67] we also performed self-consistent isodensity PCM (SCIPCM) calculations using the same basis set at the BH&HLYP level. This PCM implementation differs from the original one[52] in two ways. First, like GCOSMO (see also Hoshi et al.[68]), the solvent effects are folded directly into the Fock matrix. Second, the cavity boundary is defined by an isodensity surface which is determined self-consistently in the SCF procedure. An important feature of the SCIPCM method is that explicit atomic radii are not needed, though the free energy of solvation depends strongly on the isodensity value used. In this study, we used the suggested value of 0.001 au.[67]

All gas-phase and GCOSMO calculations were done using our locally modified Gaussian 92/DFT program[62] and SCIPCM calculations were carried out using the Gaussian 94 program.[67]

IV. Results and Discussion

A. Gas-Phase S_N2 Reaction Profile. Gas-phase geometrical parameters of the methyl chloride, $Cl^-\cdots CH_3Cl$ ion–dipole complex and S_N2 $[Cl\cdots CH_3\cdots Cl]^-$ transition state calculated at different levels of theory are listed in Table 1 along with previous theoretical results[13,14] and available experimental data.[69] In our discussion on the accuracy of different hybrid DFT methods, whenever experimental data is not availabe for comparison we used our MP2 results as a reference point. Note that the present MP2 geometries are in a good agreement with MP2 calculations using a larger basis set.[13] For the methyl chloride, all levels of theory considered here yield good agreement with experimental data. The largest structural variation between results from different methods is in the $Cl^-\cdots CH_3Cl'$ ion–dipole complex. In particular, the ion–dipole complex distance, R_{CCl}, is predicted to be 3.257 Å at the MP2 level as compared to 3.098, 3.210, and 3.193 Å at the BP, BH&HLYP, and B3LYP levels, respectively. For the D_{3h} transition state, all DFT methods predict the CCl bond distance to be larger than the MP2 result by more than 0.03 Å. Among the nonlocal DFT methods considered here, the BH&HLYP method yields slightly better agreement with the MP2 geometries and experimental data.

In this study, we found that vibrational harmonic frequencies of the methyl chloride, $Cl^-\cdots CH_3Cl$ ion–dipole complex, and S_N2 transition state calculated at both B3LYP and BH&HLYP levels agree well with the MP2 results and with available

TABLE 2: Binding Energy of the $Cl^-\cdots CH_3Cl$ Ion–Dipole Complex (ΔE_0^C) and the Classical Barrier Height (kcal/mol) of the S_N2 Reaction in the Gas Phase ($\Delta E^{\ddagger}$) and in an Aqueous Solution ($\Delta E_s^{\ddagger}$)

	HF	MP2	MP2[a]	MP4[a]	BH&HLYP	B3LYP	expt
ΔE_0^C	−9.0	−9.6	−10.5	−10.6	−9.9	−10.0	−8.6 ± 0.2[b]
$\Delta E^{\ddagger}$	6.4	7.6	3.1	1.8	2.6	−1.3	3.1[c]
$\Delta E_s^{\ddagger}$	21.5	24.3			19.2	16.0	≈26[d]

[a] Taken from ref 14. MP2 results were calculated using the TZ3P+R+(2f,d) basis set. MP4 results included the MP4 corrections calculated with the 6-31+G(d,p) basis set to the MP2/TZ3P+R+(2f,d) values. [b] Estimated from the experimental ΔH_{298}^C value.[72] Taken from ref 14. [c] From the analytical potential energy function,[12] which was fitted to the experimental rate constant at 300 K. [d] From refs 73 and 74.

experimental data particularly for equilibrium structures. This is consistent with previous findings.[70,71]

Complexation energies and barrier heights to the S_N2 reaction calculated at different levels of theory are compared with available experimental data in Table 2. Both BH&HLYP and B3LYP methods predict the complex binding energy in excellent agreement with the MP2, MP4 and G2(+) results,[13] which are about 1−2 kcal/mol too low compared to the experimental value[72] of −8.6 ± 0.2 kcal/mol. The classical barrier height, however, varies significantly for different methods. A semiempirical analytical potential energy function,[12] which was fitted to the experimental thermal rate constant[73] for this reaction at 300 K, has the classical barrier of 3.1 kcal/mol. We use this fitted value as a reference point for our discussion of the barrier height and the hydration effects below. Our MP2/6-31+G(d,p) calculations predict the barrier to be 7.6 kcal/mol and are consistent with the previous study by Tucker and Truhlar.[10] Recent MP2 calculations[13] with a much larger basis set drop this barrier to 3.1 kcal/mol. Thus, there is a large basis set dependency at this level of theory. The barrier is further reduced to 1.8 kcal/mol at the MP4 level.[13] Previous G2(+) calculations[15] predicted the zero-energy corrected barrier of 2.3 kcal/mol. Deng et al.[14] found that the VWN and BP density functionals yield the barriers of −8.9 and −5.7 kcal/mol, respectively. Negative values indicate the calculated barrier is below the separated reactants. In the present study, we found that the hybrid B3LYP method predicts the barrier to be −1.8 kcal/mol, this is much better than the VWN and BP methods, but is still too low. We found, however, that the classical BH&HLYP/6-31+G(d,p) barrier is about 2.6 kcal/mol. Including the zero-energy correction lowers the barrier to 2.2 kcal/mol. This is in excellent agreement with the semiempirical fitting and large basis set MP2, MP4, and G2(+) results. The basis-set dependence in nonlocal DFT calculations may affect such agreement and requires further studies.

In conclusion, we found that by comparison to the accurate ab initio MO calculations and available experimental data, the hybrid BH&HLYP DFT method gives the best overall performance among the considered DFT methods and can predict accurate structural, energetic, and vibrational frequency information not only for equilibrium structures but also for the transition state with quality comparable to the MP2 level of theory. This conclusion supports our previous finding on the accuracy of the BH&HLYP method for predicting transition state properties.[23,25,27]

B. Hydration Effects on the S_N2 Reaction Profile. Barrier to the S_N2 Reaction in a Solution. Classical barrier heights for the S_N2 reaction in an aqueous solution calculated at different levels of theory are listed in Table 2.[74,7] In Figure 1, we show the reaction profiles of the S_N2 reaction in both the gas phase and aqueous solution calculated at the MP2, BH&HLYP, and B3LYP levels. The calculated reaction profiles for the solution case were found to have unimodal shapes and thus are consistent with the experimental observations.[74,7] Our present results also agree with the reaction profile calculated from classical MC simulations.[30] Quantitatively, the calculated liquid-phase barriers at different levels of theory are too low by 2−10 kcal/mol with respect to the experimental estimate of 26 kcal/mol.[74,7] This error range, however, is somewhat misleading since it includes errors from the calculated gas-phase barriers. However, we can still discuss the accuracy of the GCOSMO model in representing the hydration effect on the barrier, which is the difference between the calculated barriers for the liquid- and gas-phase reactions. We found that the calculated solvent contributions to the barrier height range from 15.1 to 17.3 kcal/mol for all methods considered here as compared to the experimental value of 22.9 kcal/mol, which is estimated as the difference between the experimental liquid-phase (26 kcal/mol) and semiempirical gas-phase (3.1 kcal/mol) barriers. Thus, the present GCOSMO model underestimates the solvent contribution to the S_N2 barrier by 6−8 kcal/mol.

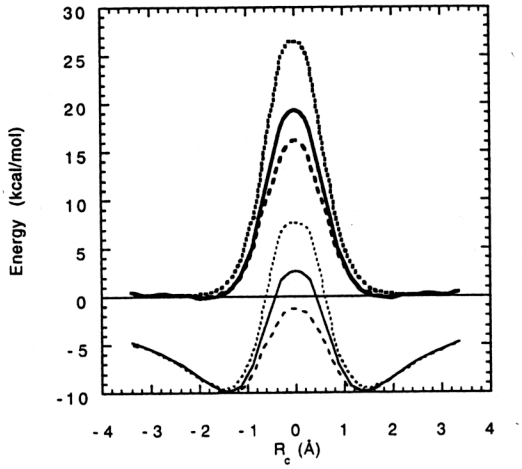

Figure 1. Reaction profiles of the S_N2 $Cl^- + CH_3Cl'$ reaction in the gas phase (thin lines) and in an aqueous solution (thick lines). Solid lines are from the BH&HLYP, dashed lines from the B3LYP, and dotted lines from the MP2 calculations using the 6-31+G(d,p) basis set.

To account for the above differences, we further analyzed the calculated hydration energies. Note that the GCOSMO model underestimates the hydration free energies of Cl^- and CH_3Cl. For instance, at the BH&HLYP level these species are less solvated than in experiment by 4.1 and 1.5 kcal/mol, respectively (see Table 3). Such large underestimation in the hydration free energy of Cl^- is due to the fact that valence electrons of the Cl anion are quite diffuse; as a result, there is a noticeable electron distribution outside the cavity. This leads to a smaller total surface charge than the value from Gauss's theorem and hence a smaller hydration free energy. Tomasi and co-workers[52] have previously proposed a surface charge renormalization procedure to address this problem. However, the physical justification for such a procedure is not clear, and thus it was not employed here.

For better understanding on the hydration effects on the activation barrier of this reaction, we decomposed the free energy of hydration into individual contributions, namely, electrostatic, dispersion, repulsion, and cavitation, and plotted these terms as functions of the reaction coordinate in Figure 2 for the BH&HLYP method. Numerical results for the reactants Cl^- and CH_3Cl, and the transition state are also listed in Table 3. We discuss below the electrostatic and nonelectrostatic contributions separately.

TABLE 3: Electrostatic and Nonelectrostatic Contributions (kcal/mol) to the Calculated Free Energy of Hydration ΔG_s

	electrostatic contribution					nonelectrostatic contributions				
	GCOSMO				SCIPCM	GCOSMO BH&HLYP				expt[a]
	HF	MP2	BH&HLYP	B3LYP	BH&HLYP	ΔG_{disp}	ΔG_{rep}	ΔG_{cav}	ΔG_s	ΔG_s
Cl^-	−74.67	−73.23	−73.74	−72.61	−57.59	−5.60	3.07	5.40	−70.87	−75
CH_3Cl	−3.09	−2.46	−2.51	−2.97	−2.97	−8.00	2.76	8.90	0.85	−0.6
$[Cl\cdots CH_3\cdots Cl]^-$	−60.66	−56.97	−57.85	−56.19	−41.25	−11.78	4.0	12.23	−53.40	
$[Cl\cdots CH_3\cdots Cl]^{-b}$	17.10	18.72	18.70	19.39	19.31	1.82	−1.83	−2.07	16.62	≈23[c]

[a] Taken from ref 7. [b] Relative to the solvation energies of the reactants, $Cl^- + CH_3Cl$. [c] Estimated from the experimental barrier for the liquid-phase reaction[73,74] and the semiempirical barrier for the gas-phase reaction.[12]

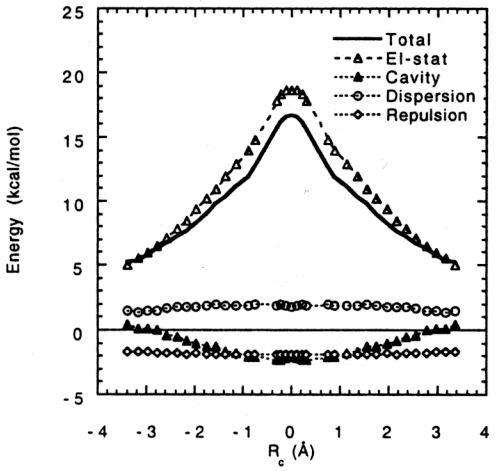

Figure 2. BH&HLYP/6-31+G(d,p) total hydration free energy (solid line) and its individual contributions (opened triangles, electrostatic; filled triangles, cavitation; circles, dispersion, diamonds, repulsion) plotted versus the reaction coordinate, R_c. All contributions are relative to their values for separated reactants.

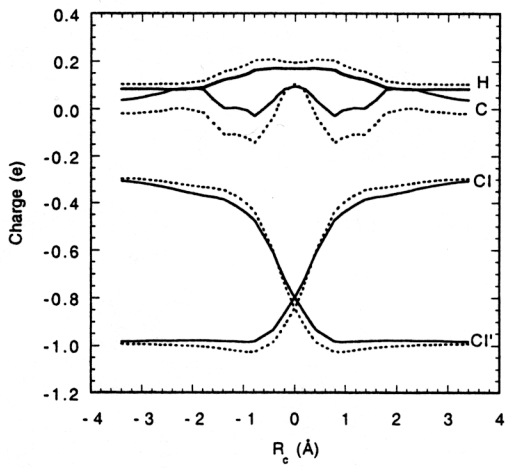

Figure 3. HF/6-31+G(d,p) calculated partial charges plotted versus the reaction coordinate, R_c. These charges were detemined from fitting to the gas-phase (solid lines) and liquid-phase (dotted lines) solute electrostatic potential.

The electrostatic contribution to the hydration free energy significantly raises the barrier of the S_N2 reaction in solution by 17−19 kcal/mol. This is due to the solute charge delocalization making the transition state less solvated compared to the Cl^- anion. In the present study, we found that the electrostatic solvation energies of reactants and transition state calculated at the BH&HLYP and B3LYP levels are within 1 kcal/mol from the MP2 values. Also, the effect of the solute electron correlation on the hydration energy is largest at the transition state, where it increases (makes more negative) the electrostatic hydration energy by 3.69, 2.18, and 4.47 kcal/mol at the MP2, BH&HLYP, and B3LYP levels, respectively.

The nonelectrostatic contributions to the hydration free energies are much smaller. Due to the small variations in geometries of CH_3Cl and the transition state at different levels of theory, the dispersion, repulsion, and cavity formation terms are slightly different. For simplicity, we listed only results for the BH&HLYP method in Table 3. Notice from Figure 2, the dispersion and repulsion terms almost cancel each other. Consequently, the overall nonelectrostatic contribution, resulting mostly from the cavity formation term, is found to lower the barrier by about 2 kcal/mol and thus would enhance the rate by a Boltzmann factor of 29 at 300 K. For reactions where the electrostatic contribution is small, such nonelectrostatic terms become important for understanding their reaction mechanisms in solution, though have often been ignored in previous dielectric continuum studies.[39,43−46,48]

Solute Electron Density Redistribution. To illustrate the effect of the solvent-induced solute electron density redistribution on the reaction profile, we used the HF-GCOSMO theory. In Figure 3, we plot two sets of partial charges as functions of the reaction coordinate, R_c. One set (solid lines) was fitted to the gas-phase and the other (dashed lines) to the liquid-phase solute electrostatic potential using the CHELPG procedure.[75] It is known that the solvent reaction field polarizes the solute electron density distribution. At the transition state, due to its high symmetry (D_{3h}), such polarization is found to be small. We found the largest effect near the ion−dipole complex, where the CH_3 group is noticeably polarized with substantial electron density from the three H atoms redistributed on the carbon atom. The electron density redistribution on the two Cl atoms is found to be smaller than that on the carbon center.

The large solute electron density redistribution found in this study raises an important question regarding the validity of using partial charges from the gas-phase electrostatic potential in many classical solvation models, including our classical GCOSMO model.[9] In these models, the reaction profile in solution is usually calculated by adding the classical solvation energy to the quantum gas-phase reaction profile, thus neglecting the effect of the solvent-induced electron density redistribution. To estimate the magnitude of this error, we have calculated the liquid-phase S_N2 reaction profiles with the classical GCOSMO model using either the gas-phase or liquid-phase partial charges. As shown in Figure 4, using the gas-phase partial charges yields an error of about 3 kcal/mol in the S_N2 barrier relative to the full quantum results. When using the liquid-phase partial charges this error is reduced to about 1.5 kcal/mol. Note that such an error is still comparable to the nonelectrostatic solvation energies.

Finally, we studied the validity of using the gas-phase geometries for calculating the reaction profile of this S_N2 reaction in solution. For this purpose, we performed geometry optimization for both the reactants and transition state using analytical energy gradients derived for the GCOSMO model.[51] We found that the solvent reaction field has a small effect (less than 0.005 Å) on the geometries of CH_3Cl and the transition

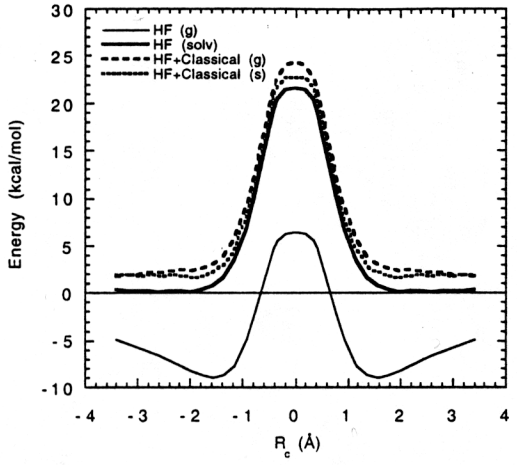

Figure 4. HF/6-31G+G(d,p) reaction profiles for the gas-phase (lower solid line) and liquid-phase (upper lines) S_N2 $Cl^- + CH_3Cl$ reactions. Upper solid line is from the full quantum HF-GCOSMO calculation, dashed line is from the HF gas-phase energies plus classical hydration energies calculated from the gas-phase partial charges, and dotted line is similar to the dashed line except the liquid-phase partial charges were used.

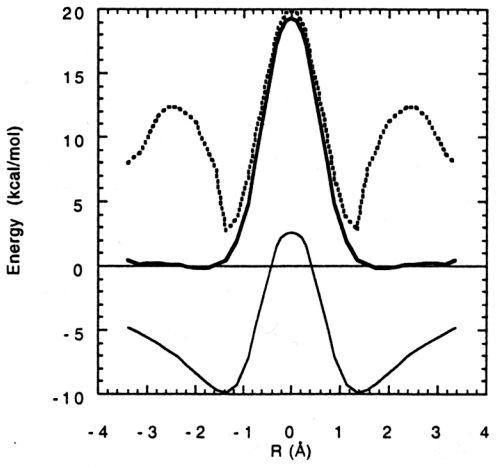

Figure 5. BH&HLYP/6-31+G(d,p) reaction profiles for the gas-phase (lower solid line) and liquid-phase (upper lines) S_N2 $Cl^- + CH_3Cl$ reactions. Upper solid line is from GCOSMO results, upper dashed line is from SCIPCM calculations.

state and thus yields a negligible change (less than 0.1 kcal/mol) in the calculated barrier height.

C. Performance of GCOSMO and SCIPCM Methods. In our previous study,[9] we found that the GCOSMO method can achieve an accuracy on the order of 2 kcal/mol for neutral molecules and 4−5 kcal/mol for molecular ions. Our present results are consistent with this finding. Our recent results indicate that we can improve the accuracy of the GCOSMO method by systematically optimizing atomic radii at ab initio levels of theory to experimental hydration free energies of a set of neutral polar and nonpolar molecules and ions. We discuss the fitting of atomic radii in a separate report.[76]

One of the main criticisms of dielectric continuum solvation models is the arbitrariness of the atomic radii used. The SCIPCM method introduced recently in the Gaussian 94 program offers an alternative for defining the cavity by a single parameter, the isodensity value. To test the accuracy of this method, we have performed BH&HLYP-SCIPCM electrostatic calculations using the same 6-31+G(d,p) basis set as above and added the nonelectrostatic contributions obtained with the use of the BH&HLYP-GCOSMO algorithm. Although the SCIPCM model predicts the reaction barrier of 19.8 kcal/mol in good agreement with GCOSMO results and experimental data, the SCIPCM hydration free energies for the Cl anion and S_N2 transition state are strongly underestimated (see Table 3). A more dramatic difference between GCOSMO and SCIPCM models is in the calculated reaction profile as shown in Figure 5. Near the transition state, both methods agree very well, however, at R_c values of 2−3 Å the SCIPCM model yields an erroneous second barrier. The appearance of this barrier can be explained by an abrupt decrease of the hydration free energy of the complex. At $R_c > 1$ the electron density redistributes from the methyl chloride Cl atom to the leaving Cl'^- ion (see Figure 3). This redistribution is accompanied with the inflation of the isodensity contour around Cl'^- that decreases the hydration free energy of this anion which is the major component of the total ΔG_s. Additional studies and testing on the accuracy and applicability of the GCOSMO and SCIPCM methods for calculation of the hydration free energies and the reaction profiles in solutions are currently being performed in our lab.

V. Conclusion

In this study, we have carried out a theoretical study of the hydration effects on the reaction profile of the S_N2 $Cl^- + CH_3Cl$ reaction using our recently proposed GCOSMO model. Reaction profiles in both gas phase and liquid phase were calculated using the HF, MP2, and nonlocal hybrid DFT methods with the 6-31+G(d,p) basis set. On the basis of these results, we are able to formulate three conclusions:

(1) From a point of view of new methodological development, rather good correspondence between MP2 and DFT results for hydration effects on reaction profiles is very encouraging. Particularly, due to the computational advantage of the DFT methods for large systems, applications of the GCOSMO continuum solvation model within the DFT formalism for quantitative studies on dynamics and mechanisms of chemical and biochemical reactions in solutions are now feasible. The BH&HLYP method gives the overall best performance for predicting geometrical, energetic, and frequency information at both the reactants and transition state.

(2) The GCOSMO model was found to predict reasonably accurate hydration effects on the reaction profile of this S_N2 reaction. Particularly for this reaction, we found that the calculated reaction profile in solution is unimodal, which is consistent with the experimental suggestion and previous MC simulations. On the other hand, the SCIPCM model was found to significantly underestimate the hydration free energies of anions and yield incorrect features on the liquid-phase reaction profile.

(3) The calculated gas-phase S_N2 reaction barrier is very sensitive to the method of treating the correlation effects. We estimated contributions of different effects to the S_N2 reaction barrier in water: (a) the most important contribution to the barrier height (about 19 kcal/mol) is due to the electrostatic hydration energy; (b) the intrasolute electron correlation increases the barrier by 1.5−2.2 kcal/mol; (c) the solvent-induced electron density redistribution in the solute decreases the barrier by 1.5−3.0 kcal/mol; (d) the nonelectrostatic hydration effects decrease the barrier by about 2 kcal/mol; (e) the solvent-induced geometry changes of the solute are small and correspond to changes in the energy of less than 0.1 kcal/mol.

Acknowledgment. This work was supported in part by the University of Utah and the National Science Foundation through a Young Investigator Award to T.N.T.

References and Notes

(1) Ingold, C. K. *Structure and Mechanism in Organic Chemistry*, 2nd ed.; Cornell University Press: Ithaca, NY, 1969.

(2) Hynes, J. T. The theory of reactions in solution. In *Theory of Chemical Reaction Dynamics*; Baer, M., Ed.; CRC Press: Boca Raton, FL, 1985; Vol. 4, p 171.

(3) Kreevoy, M. M.; Truhlar, D. G. Transition State Theory. In *Investigation of Rates and Mechanisms of Reactions*, 4th ed.; Bernasconi, C. F., Ed.; John Wiley & Sons: New York, 1986; Vol. I; p 13.

(4) Minkin, V. I.; Simkin, B. Y.; Minyaev, R. M. *Quantum Chemistry of Organic Compounds-Mechanisms of Reactions*; Springer-Verlag: Berlin, 1990.

(5) Shaik, S. S.; Schlegel, H. B.; Wolfe, S. *Theoretical Aspects of Physical Organic Chemistry, The S_N2 Mechanisms*; Wiley: New York, 1992.

(6) Olmstead, W. N.; Brauman, J. I. *J. Am. Chem. Soc.* **1977**, *99*, 4219.

(7) Albery, W. J. *Annu. Rev. Phys. Chem.* **1980**, *31*, 227.

(8) Stefanovich, E. V.; Truong, T. N. *J. Comput. Chem.*, submitted.

(9) Truong, T. N.; Stefanovich, E. V. *Chem. Phys. Lett.* **1995**, *240*, 253.

(10) Tucker, S.; Truhlar, D. G. *J. Phys. Chem.* **1989**, *93*, 8138.

(11) Vande Linde, S. R.; Hase, W. L. *J. Am. Chem. Soc.* **1989**, *111*, 2349.

(12) Tucker, S. C.; Truhlar, D. G. *J. Am. Chem. Soc.* **1990**, *112*, 3338.

(13) Wladkowski, B. D.; Lim, K. F.; Allen, W. D.; Brauman, J. I. *J. Am. Chem. Soc.* **1992**, *114*, 9136.

(14) Deng, L.; Branchadell, V.; Ziegler, T. *J. Am. Chem. Soc.* **1994**, *116*, 10645.

(15) Glukhovtsev, M. N.; Pross, A.; Radom, L. *J. Am. Chem. Soc.* **1995**, *117*, 2024.

(16) Vosko, S. H.; Wilk, L.; Nusair, M. *Can. J. Phys.* **1980**, *58*, 1200.

(17) Becke, A. D. *Phys. Rev. A* **1988**, *38*, 3098.

(18) Perdew, J. P. *Phys. Rev. B* **1986**, *33*, 8822.

(19) Becke, A. D. *J. Chem. Phys.* **1993**, *98*, 5648.

(20) Lee, C.; Yang, W.; Parr, R. G. *Phys. Rev. B* **1988**, *37*, 785.

(21) Becke, A. D. *J. Chem. Phys.* **1993**, *98*, 1372.

(22) Abashkin, Y.; Russo, N. *J. Chem. Phys.* **1994**, *100*, 4477.

(23) Bell, R.; Truong, N. T. *J. Chem. Phys.* **1994**, *101*, 10442.

(24) Stanton, R. V.; Merz, K. M., Jr. *J. Chem. Phys.* **1994**, *100*, 434.

(25) Truong, T. N.; Duncan, W. T. *J. Chem. Phys.* **1994**, *101*, 7408.

(26) Baker, J.; Andzelm, J.; Muir, M.; Taylor, P. R. *Chem. Phys. Lett.* **1995**, *237*, 53.

(27) Zhang, Q.; Bell, R.; Truong, T. N. *J. Phys. Chem.* **1995**, *99*, 592.

(28) Morokuma, K. *J. Am. Chem. Soc.* **1982**, *104*, 3732.

(29) Shaik, S. S. *J. Am. Chem. Soc.* **1984**, *106*, 1227.

(30) Chandrasekhar, J.; Smith, S. F.; Jorgensen, W. L. *J. Am. Chem. Soc.* **1985**, *107*, 154.

(31) Singh, U. C.; Kollman, P. A. *J. Comput. Chem.* **1986**, *7*, 718.

(32) Bash, P. A.; Field, M. J.; Karplus, M. *J. Am. Chem. Soc.* **1987**, *109*, 8092.

(33) Burshtein, K. Y. *J. Mol. Struc. (THEOCHEM)* **1987**, *153*, 209.

(34) Hwang, J.-K.; Creighton, S.; King, G.; Whitney, D.; Warshel, A. *J. Chem. Phys.* **1988**, *89*, 859.

(35) Hwang, J.-K.; King, G.; Creighton, S.; Warshel, A. *J. Am. Chem. Soc.* **1988**, *110*, 5297.

(36) Alemán, C.; Maseras, F.; Lledós, A.; Duran, M.; Bertrán, J. *J. Phys. Org. Chem.* **1989**, *2*, 611.

(37) Huston, S. E.; Rossky, P. J.; Zichi, D. A. *J. Am. Chem. Soc.* **1989**, *111*, 5680.

(38) Jorgensen, W. L. *Acc. Chem. Res.* **1989**, *22*, 184.

(39) Kozaki, T.; Morihashi, K.; Kikuchi, O. *J. Am. Chem. Soc.* **1989**, *111*, 1547.

(40) Tucker, S. C.; Truhlar, D. G. *J. Am. Chem. Soc.* **1990**, *112*, 3347.

(41) Gertner, B. J.; Whitnell, R. M.; Wilson, K. R.; Hynes, J. T. *J. Am. Chem. Soc.* **1991**, *113*, 74.

(42) Gonzalez-Lafont, A.; Truong, T. N.; Truhlar, D. G. *J. Phys. Chem.* **1991**, *95*, 4618.

(43) Bianco, R.; Miertuš, S.; Persico, M.; Tomasi, J. *Chem. Phys.* **1992**, *168*, 281.

(44) Ford, G. P.; Wang, B. *J. Am. Chem. Soc.* **1992**, *114*, 10563.

(45) Aguilar, M.; Bianco, R.; Miertuš, S.; Persico, M.; Tomasi, J. *Chem. Phys.* **1993**, *174*, 397.

(46) Basilevsky, M. V.; Chudinov, G. E.; Napolov, D. V. *J. Phys. Chem.* **1993**, *97*, 3270.

(47) Mathis, J. R.; Bianco, R.; Hynes, J. T. *J. Mol. Liq.* **1994**, *61*, 81.

(48) Sato, H.; Kato, S. *J. Mol. Struc. (THEOCHEM)* **1994**, *310*, 67.

(49) Luzhkov, V.; Warshel, A. *J. Comput. Chem.* **1992**, *13*, 199.

(50) Klamt, A.; Schüürmann, G. *J. Chem. Soc., Perkin Trans. 2* **1993**, 799.

(51) Truong, T. N.; Stefanovich, E. V. *J. Chem. Phys.*, in press.

(52) Miertuš, S.; Scrocco, E.; Tomasi, J. *Chem. Phys.* **1981**, *55*, 117.

(53) Fortunelli, A.; Tomasi, J. *Chem. Phys. Lett.* **1994**, *231*, 34.

(54) Chen, J. L.; Noodleman, L.; Case, D. A.; Bashford, D. *J. Phys. Chem.* **1994**, *98*, 11059.

(55) Rashin, A. A.; Bukatin, M. A.; Andzelm, J.; Hagler, A. T. *Biophys. Chem.* **1994**, *51*, 375.

(56) Tannor, D. J.; Marten, B.; Murphy, R.; Friesner, R. A.; Sitkoff, D.; Nicholls, A.; Ringnalda, M.; Goddard, W. A.; Honig, B. *J. Am. Chem. Soc.* **1994**, *116*, 11875.

(57) Richards, F. M. *Annu. Rev. Biophys. Bioeng.* **1977**, *6*, 151.

(58) Floris, F. M.; Tomasi, J.; Ahuir, J. L. P. *J. Comput. Chem.* **1991**, *12*, 784.

(59) Jorgensen, W. L.; Tirado-Rives, J. *J. Am. Chem. Soc.* **1988**, *110*, 1657.

(60) Pierotti, R. A. *Chem. Rev.* **1976**, *76*, 717.

(61) Huron, M. J.; Claverie, P. *J. Phys. Chem.* **1972**, *76*, 2123.

(62) Frisch, M. J.; Trucks, G. W.; Schlegel, H. B.; Gill, P. M. W.; Johnson, B. G.; Wong, M. W.; Foresman, J. B.; Robb, M. A.; Head-Gordon, M.; Replogle, E. S.; Gomperts, R.; Andres, J. L.; Raghavachari, K.; Binkley, J. S.; Gonzalez, C.; Martin, R. L.; Fox, D. J.; Defrees, D. J.; Baker, J.; Stewart, J. J. P.; Pople, J. A., Gaussian 92/DFT, Revision G.3; Gaussian, Inc.: Pittsburgh, 1993.

(63) Rashin, A. A.; Namboodiri, K. *J. Phys. Chem.* **1987**, *91*, 6003.

(64) Hagler, A. T.; Huler, E.; Lifson, S. *J. Am. Chem. Soc.* **1973**, *96*, 5319.

(65) Brooks, B. R.; Bruccoleri, R. E.; Olafson, B. D.; States, D. J.; Swaminathan, S.; Karplus, M. *J. Comput. Chem.* **1983**, *4*, 187.

(66) Pascual-Ahuir, J. L.; Silla, E.; Tuñon, I. *J. Comput. Chem.* **1994**, *15*, 1127.

(67) Frisch, M. J.; Trucks, G. W.; Schlegel, H. B.; Gill, P. M. W.; Johnson, B. G.; Robb, M. A.; Cheeseman, J. R.; Keith, T. A.; Petersson, G. A.; Montgomery, J. A.; Raghavachari, B.; Al-Laham, M. A.; Zakrzewski, V. G.; Ortiz, J. V.; Foresman, J. B.; Cioslowski, J.; Stefanov, B.; Nanayakkara, A.; Challacombe, M.; Peng, C. Y.; Ayala, P. Y.; Chen, W.; Wong, M. W.; Andres, J. L.; Replogle, E. S.; Gomperts, R.; Martin, R. L.; Fox, D. J.; Binkley, J. S.; Defrees, D. J.; Baker, J.; Stewart, J. P.; Head-Gordon, M.; Gonzalez, C.; Pople, J. A. Gaussian 94, Revision B.1; Gaussian, Inc.: Pittsburgh, 1995.

(68) Hoshi, H.; Chûjô, R.; Inoue, Y.; Sakurai, M. *J. Chem. Phys.* **1987**, *87*, 1107.

(69) *CRC Handbook of Chemistry and Physics*, 74th ed.; Lide, P. R., Ed.; CRC Press: Boca Raton, FL, 1993.

(70) Andzelm, J.; Wimmer, E. *J. Chem. Phys.* **1992**, *96*, 1280.

(71) Johnson, B. G.; Gill, P. M. W.; Pople, J. A. *J. Chem. Phys.* **1993**, *98*, 5612.

(72) Larson, J. W.; McMahon, T. B. *J. Am. Chem. Soc.* **1985**, *107*, 766.

(73) Barlow, S. E.; Van Doren, J. M.; Bierbaum, V. M. *J. Am. Chem. Soc.* **1988**, *110*, 7240.

(74) Albery, W. J.; Kreevoy, M. M. *Adv. Phys. Org. Chem.* **1978**, *16*, 87.

(75) Breneman, C. M.; Wiberg, K. B. *J. Comput. Chem.* **1990**, *11*, 361.

(76) Stefanovich, E. V.; Truong, T. N. *Chem. Phys. Lett.*, in press.

JP951591W